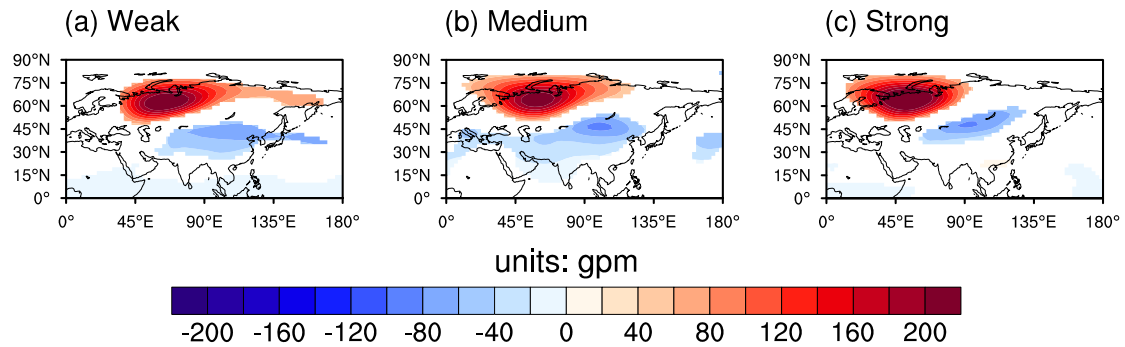
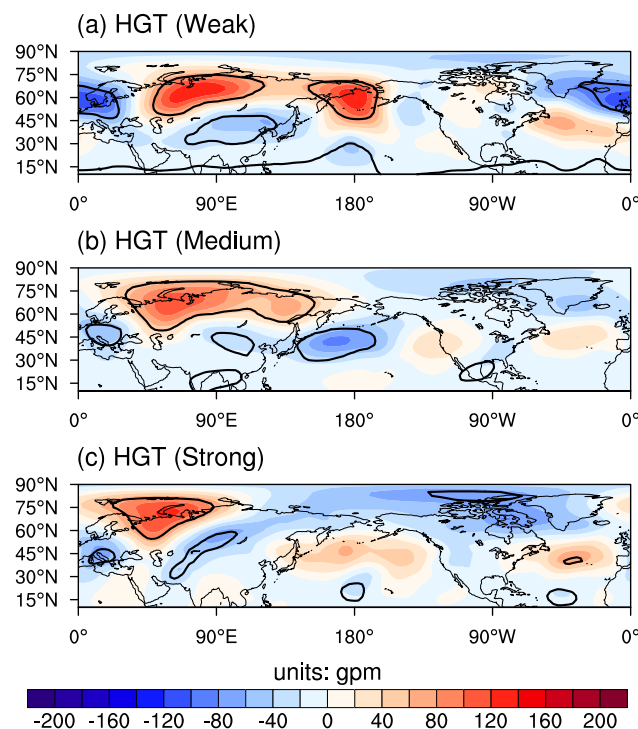


# Supplementary Materials: Ural Blocking and the Amplitude of Wintertime Cold Surges over North China Detected by a Cooling Algorithm

Zifan Yang <sup>1,\*</sup>, Wenyu Huang <sup>2</sup>, Ruyan Chen <sup>2</sup>, Daiyu Lin <sup>2</sup>, Bin Wang <sup>2</sup> and Wenqian Ma <sup>2</sup>



**Figure S1.** Composited mean daily geopotential height anomalies (units: gpm) during blocking events belonging to (a) the weak group, (b) the medium group, and (c) the strong group. The blocking events shown are constructed from the JRA55 reanalysis product over DJFM 1958-2021. The composited values are tested against the remaining days during DJFM 1958-2021 based on two-tailed Student's *t* tests. Only composited values that are significant at the 95% confidence level are plotted.



**Figure S2.** The composited mean geopotential height anomalies (units: gpm) over the Northern Hemisphere three days prior to the onset of the cooling event associated with each blocking event. Results are estimated for the (a) weak group, (b) medium group, and (c) strong group cooling events based on JRA55. The composited values are tested against the remaining days during DJFM 1958-2021 based on two-tailed Student's *t* tests and only composited values that pass the 95% confidence level are enclosed by solid contour lines.

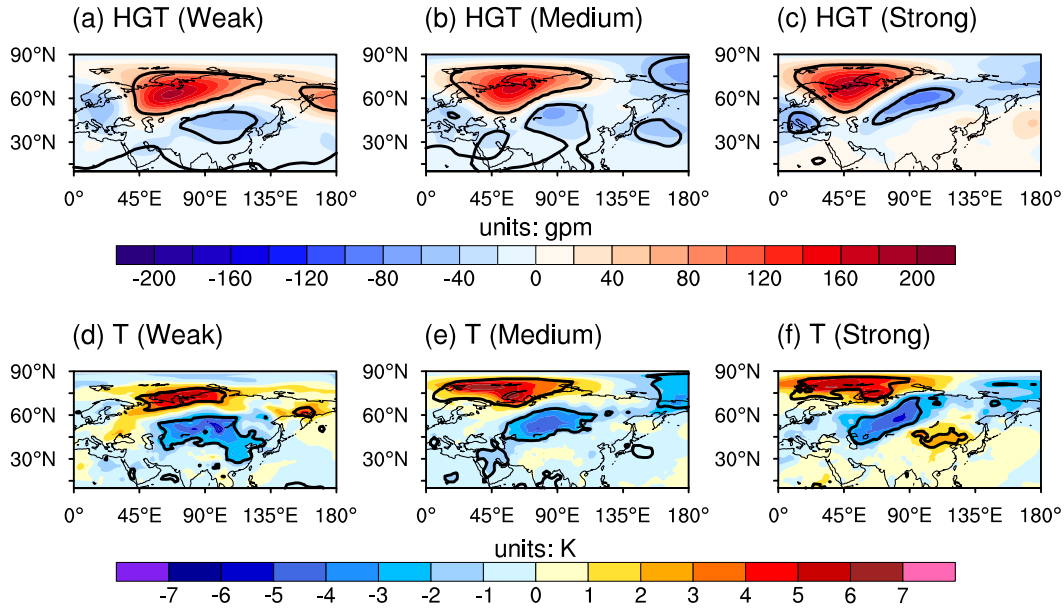


**Figure S3.** The composited mean (a-c) geopotential height anomalies (units: gpm) and (d-f) surface temperature anomalies (units: K) three days prior to the onset of the cooling event associated with each blocking event. Results are estimated for the (a, d) weak group, (b, e) medium group, and (c, f) strong group cooling events based on NCEP-NCAR. The composited values are tested against the remaining days during DJFM 1948-2021 based on two-tailed Student's  $t$  tests. Composited values that are significant at the 95% confidence level are enclosed by solid contour lines.

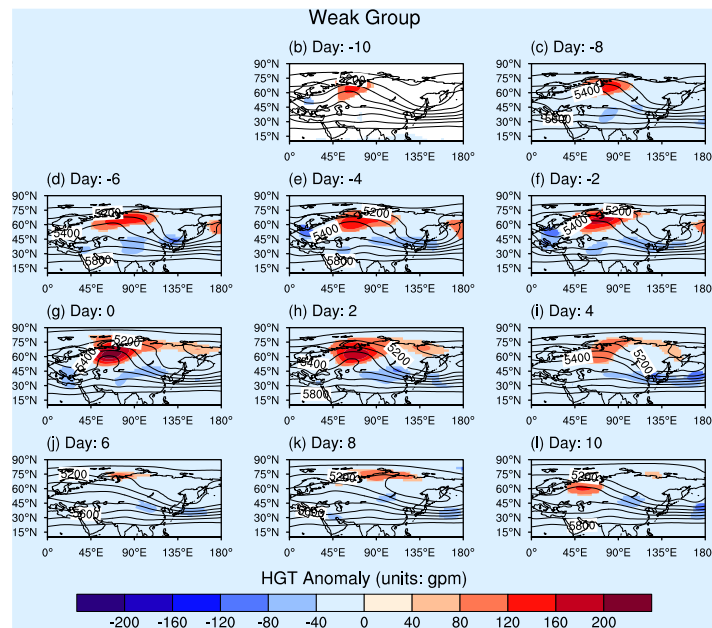


**Figure S4.** Time sequence of the composited geopotential height (contour; units: gpm) and its anomalies (shaded; units: gpm) from day -12 to day 10 (with an interval of 2 days) for the weak group cooling events constructed based on JRA55. Note that day 0 marks the onset of the cooling events associated with blocking events belonging to the weak group. The composited values are tested against the remaining days during DJFM 1958-2021 based on two-tailed Student's  $t$  tests. Only composited values that are significant at the 95% confidence level are plotted.

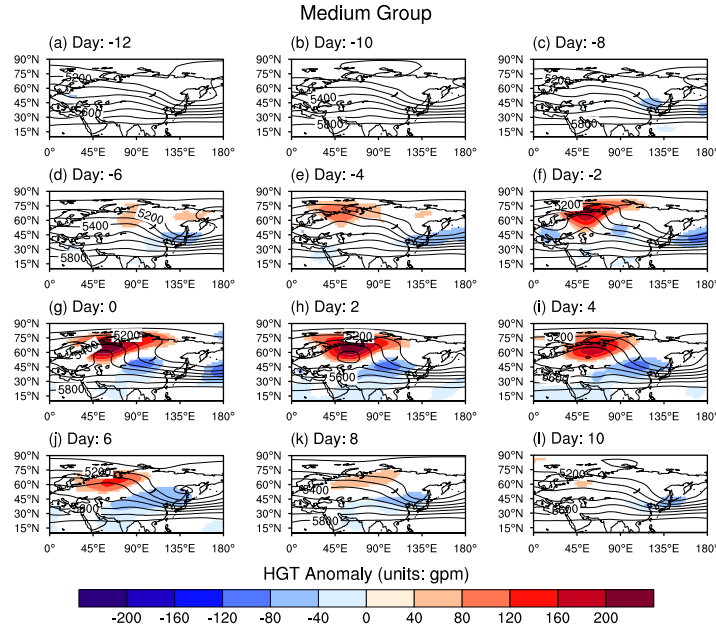


**Figure S5.** Time sequence of the composited geopotential height (contour; units: gpm) and its anomalies (shaded; units: gpm) from day -12 to day 10 (with an interval of 2 days) for the medium group cooling events constructed based on JRA55. Note that day 0 marks the onset of the cooling events associated with blocking events belonging to the medium group. The composited values are tested against the remaining days during DJFM 1958-2021 based on two-tailed Student's  $t$  tests. Only composited values that are significant at the 95% confidence level are plotted.

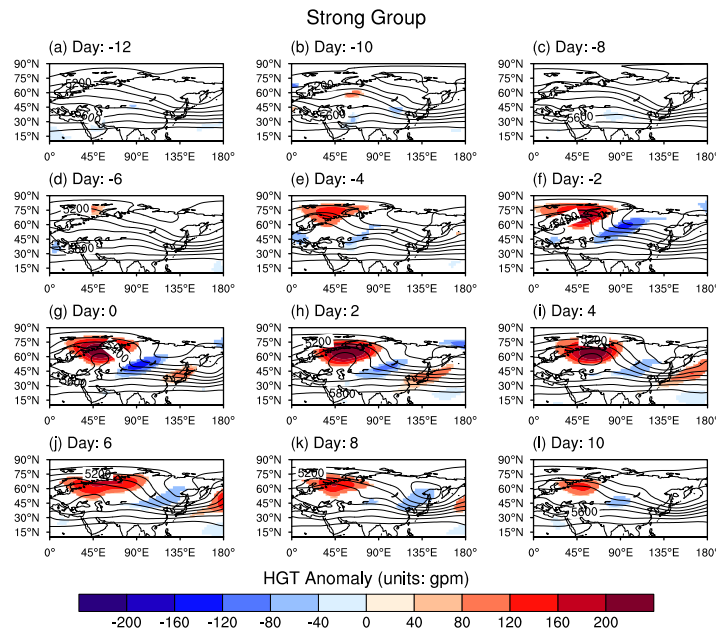


**Figure S6.** Time sequence of the composited geopotential height (contour; units: gpm) and its anomalies (shaded; units: gpm) from day -12 to day 10 (with an interval of 2 days) for the strong group cooling events constructed based on JRA55. Note that day 0 marks the onset of the cooling events associated with blocking events belonging to the strong group. The composited values are tested against the remaining days during DJFM 1958-2021 based on two-tailed Student's  $t$  tests. Only composited values that are significant at the 95% confidence level are plotted.

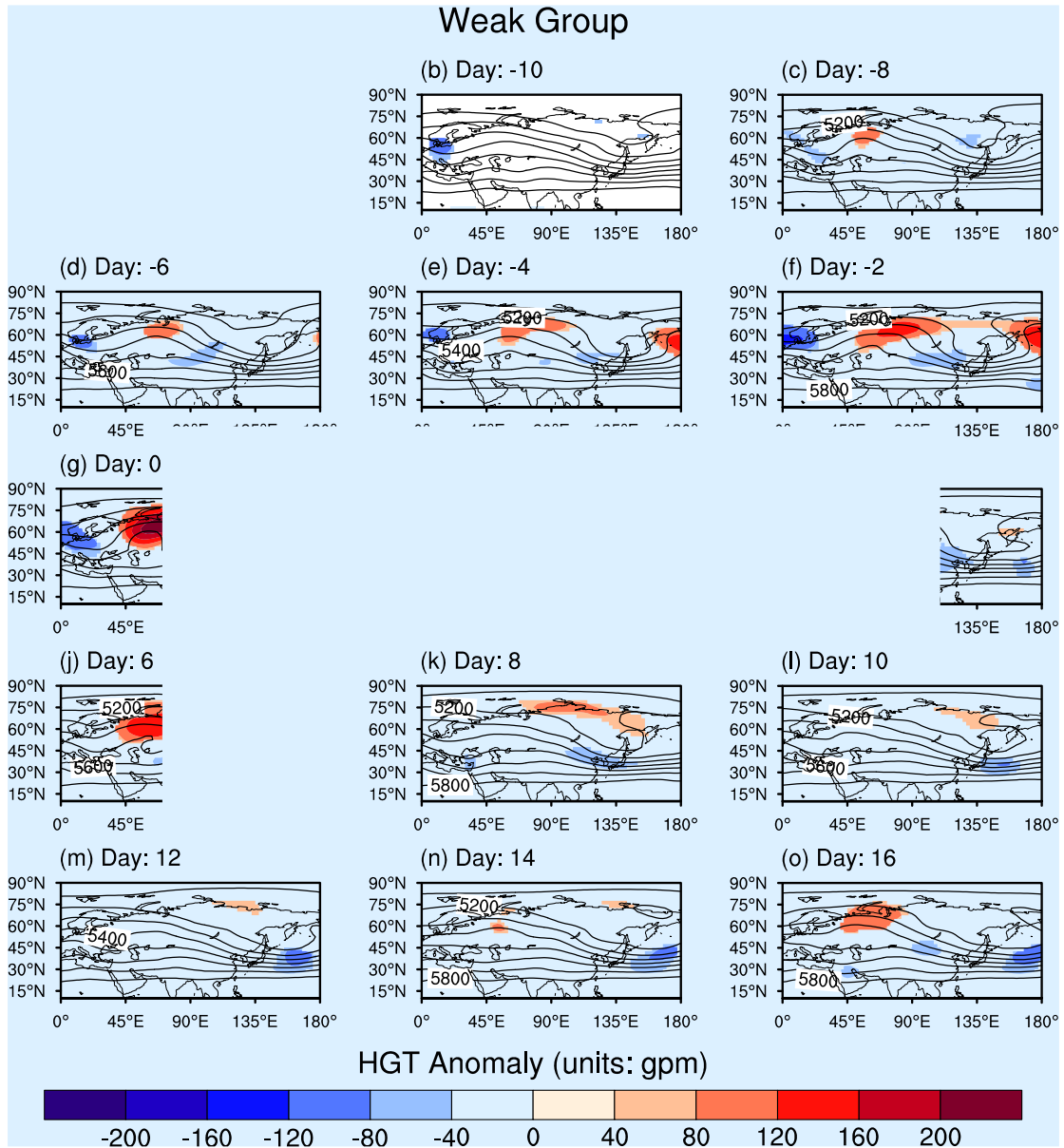


**Figure S7.** Time sequence of the composited geopotential height (contour; units: gpm) and its anomalies (shaded; units: gpm) from day -12 to day 16 (with an interval of 2 days) for the blocking events associated with weak group cooling events constructed based on JRA55. Note that day 0 marks the onset of the blocking events belonging to the weak group. The composited values are tested against the remaining days during DJFM 1958-2021 based on two-tailed Student's  $t$  tests. Only composited values that are significant at the 95% confidence level are plotted.

## Medium Group

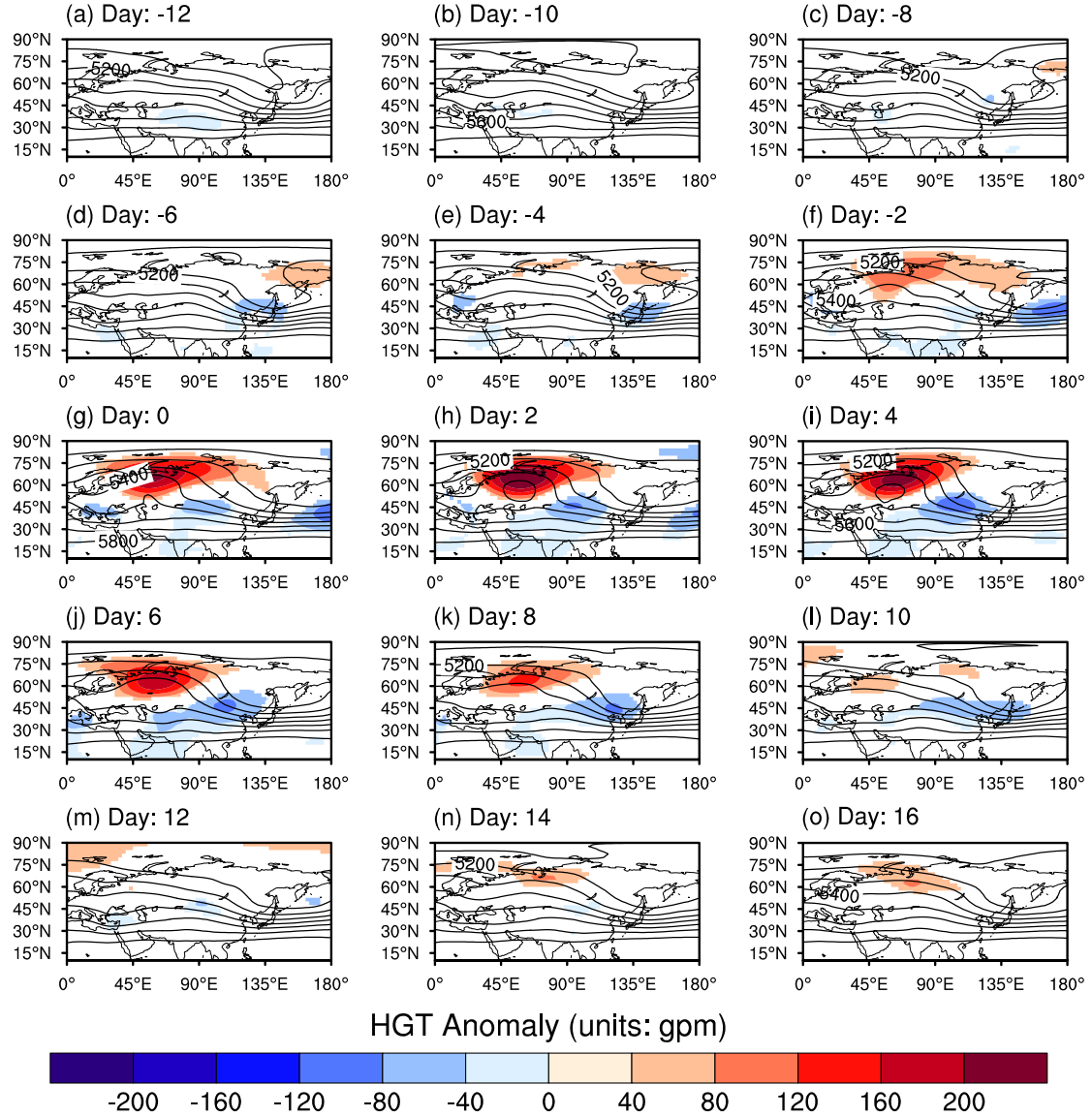


**Figure S8.** Time sequence of the composited geopotential height (contour; units: gpm) and its anomalies (shaded; units: gpm) from day -12 to day 16 (with an interval of 2 days) for the blocking events associated with medium group cooling events constructed based on JRA55. Note that day 0 marks the onset of the blocking events belonging to the medium group. The composited values are tested against the remaining days during DJFM 1958-2021 based on two-tailed Student's  $t$  tests. Only composited values that are significant at the 95% confidence level are plotted.



## Strong Group

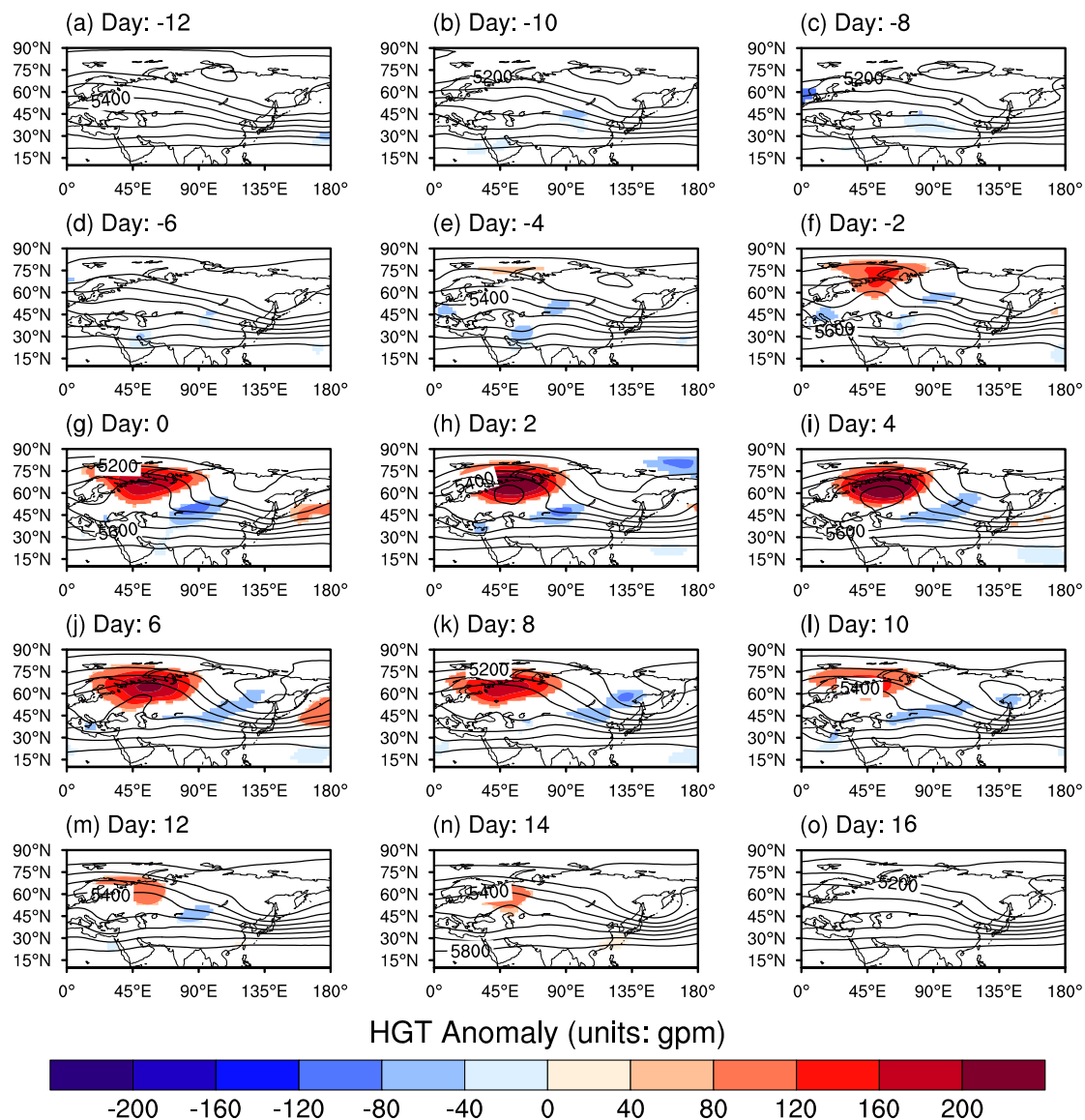


**Figure S9.** Time sequence of the composited geopotential height (contour; units: gpm) and its anomalies (shaded; units: gpm) from day -12 to day 16 (with an interval of 2 days) for the blocking events associated with strong group cooling events constructed based on JRA55. Note that day 0 marks the onset of the blocking events belonging to the strong group. The composited values are tested against the remaining days during DJFM 1958-2021 based on two-tailed Student's  $t$  tests. Only composited values that are significant at the 95% confidence level are plotted.

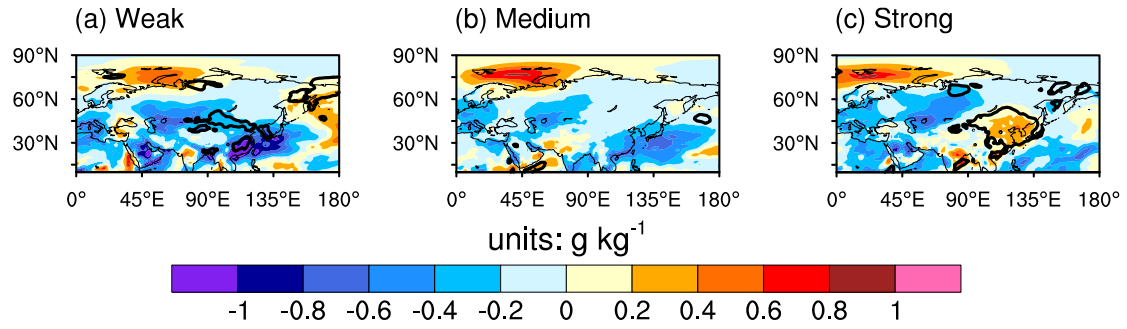


**Figure S10.** The composited mean of specific humidity (units:  $\text{g kg}^{-1}$ ) three days prior to the onset of the cooling event associated with each blocking event. Results are estimated for (a) the weak group, (b) the medium group, and (c) the strong group based on JRA55. The composited values are tested against the days belonging to the other two groups based on two-tailed Student's  $t$  tests. Composited values that are significant at the 95% confidence level are enclosed by solid contour lines.